TECHNICAL ARTICLE

Flux-Cored Wire for Arc Additive Manufacturing of Alloy Steel: Effect of Inclusion Particles on Microstructure and Properties

Min Zhang, Shuai Xu, Qiaoling Chu, Boyu Wang, Lisheng Zhang, Xiaoyu He, Xiongwei Tong, and Lin Zhang

Wire and arc additive manufacturing technology is an efficient manufacturing method to realize rapid prototyping of complex parts. Unlike most recent researches which mainly focus on the manufacturing process and equipment, this paper reports the findings of experiments in which the self-developed flux-cored wire is used for arc additive manufacturing of alloy steel. It studies the effects of the contents of inclusions forming elements Ti and Mn on the microstructure and properties of wall parts, and discusses the microstructure evolution in the manufacturing process. It is discovered that the grain size of alloy steel parts manufactured by arc additive is affected by the number of heterogeneous nucleation cores dominated by inclusions in the molten pool, resulting in changed performance of the samples. During the manufacturing process, different sections of the samples experience different thermal cycles. The central region of the sample is heated and tempered, the microstructure change from granular bainite and acicular ferrite into tempered bainite and massive ferrite, and its hardness decrease. Furthermore, the electron backscatter diffraction analysis shows that the thermal cycle makes for the recrystallization in the middle region of the sample, but plasticity of the material does not change. The mechanical properties of the samples do not show obvious anisotropy with decrease in the grain size. Therefore, this study is of particularly significance in developing raw materials for arc additive manufacturing.

1. Introduction

Wire and arc additive manufacturing (WAAM) technology is a rapid prototyping manufacturing technology, and it reduces time and procedures in manufacturing complex parts. Due to its high accumulation efficiency and material utilization (Ref 1-3), WAAM has been widely applied to equipment manufacturing in aerospace, machinery and medicine industry (Ref 1, 4, 5). Compared with the traditional manufacturing technology, WAAM technology uses welding wire as raw material so that the formed parts have dense microstructure which will improve performance of complex parts (Ref 6, 7). The arc additive manufacturing process mainly involves plasma arc welding, gas tungsten electrode protection welding, and gas metal protection welding which includes cold metal transfer (CMT) (Ref 7-10).

As a matter of fact, arc additive manufacturing technology has attracted much attention from researchers who have worked on the forming quality (Ref 11) and mechanical properties (Ref 12) of arc additive manufactured parts, especially the process

parameters (Ref 10, 13), path optimization (Ref 14) and process control (Ref 15). It is discovered that the forming quality of arc additive manufactured parts is closely related to multiple parameters in the manufacturing process, such as welding speed, wire feeding speed, and interlayer temperature. Moreover, in the MAG-based (Metal Active Gas Arc Welding) additive manufacturing process, the interlayer temperature, wire feeding speed, and welding speed produce an effect on the surface roughness of wall parts (Ref 16). And selection of printing paths and parameter control in the building process also contribute to the forming quality of wire arc additive manufacturied parts (Ref 17). Whether WAAM can be widely used in manufacturing large structures depends on the optimal performance of the formed parts. Philip Dirisu et al. (Ref 18) from Cranfield University have tried ER70S-6, ER90S-B3, ER120S-G wires in manufacturing alloy steel by arc additive, and they studied the impact of wire composition and deposition path on fracture toughness of high-strength low-alloy steel structures (HSLASS). Their research proves that the microstructure and mechanical properties of arc additive manufactured parts are closely related to composition of raw materials. In addition, other researches on serious heat accumulation and complex thermal cycle process (Ref 19) reveal that change of microstructure and performance of parts are affected by the thermal process. Different heat input (Ref 20) and cooling rates (Ref 21) can yield different phase compositions and phase ratios in the mcrostructure of arc additive manufactured parts. The complex thermal process may even lead to anisotropy of mechanical properties which cannot be eliminated by adjusting the process path but through certain post-processing methods, such as heat treatment (Ref 22) and

Min Zhang, Shuai Xu, Qiaoling Chu, Boyu Wang, Lisheng Zhang, Xiaoyu He, Xiongwei Tong, and Lin Zhang, School of Materials Science and Engineering, Xi'an University of Technology, Xi'an 710048, China. Contact e-mail: zhmmn@xaut.edu.cn.

plastic deformation. However, process adjustment has a very limited effect on adjusting microstructure and properties of arc additive manufactured parts. For example, the cladding efficiency of arc additive manufacturing may be reduced when the heat input is reduced. In other words, extra post-processing delays the manufacturing process and increases the cost of parts manufacturing.

Although the existing researches use welding materials in arc additive manufacturing, few studies have reported development of new raw materials for additive manufacturing. In the current research, we attempt at developing new raw materials for arc additive manufacturing and calfifying the impact of the raw material composition on the performance of arc additive manufactured parts by using three groups of self-designed flux-cored wire in arc additive manufacturing alloy steel. This paper illutrates our experiments on raw materials, the microstructure transformation of arc additive manufactured parts under the thermal cycle and the test results of parts performance.

2. Experiments: Materials and Process

In our experiment, the equipment for arc additive manufacturing consists of a Panasonic TM-1400G III welding robot and a YD-500GL-W welding power supply, as shown in Fig. 1. The platform can print various shapes of parts such as the wall, cylinder, and other complex structures. The minimum adjustment unit of stacking speed is 0.01 mm/min, and the minimum adjustment unit of height lifting is 0.2 mm.

2.1 Selected Materials

The wire for arc additive is a self-made flux-cored wire made up of a steel strip and flux core. The metal powder is wrapped by a A283GRC low carbon steel strip of a size 7×0.3 mm. The proportion of the metal powder in the flux-cored wire is about 21-23 wt.%, and the diameter of the flux-cored wire is 1.2 mm. The compositions of the alloy powder in flux-cored wires of the three groups are shown in Table 1, in which the content of Ti and Mn alloy elements are variables and the 1#, 2#, and 3# wires vary with the increasing contents of Ti and Mn. The Ti-Fe and Al-Mg described in Table 1 are the names of the alloy powders, and the specific composition content is shown in Table 2.

The substrate is made of $200 \times 200 \times 10$ mm A283GRC low carbon steel and its chemical composition is shown in Table 3. In preparation for stacking in the experiment, the substrate surface needs to be polished and cleaned with anhydrous ethanol to avoid oxide and oil pollution in the welding process.

2.2 WAAM Process

In accordance with ANSI/AWS A5.32M/A5.32:2011, we use 90% Ar + 10% CO_2 as welding protective gas at a flow rate of 15L/min. The wire extends 10 mm long, and the wall is printed along a linear path with180 mm in length and 70 mm in height. In our previous process parameters tests, the process parameters for printing wall parts with the flux-cored wire are: current 165-175 A, voltage 21-23 V, welding speed 21 mm/min. In the printing process of wall parts, the interlayer temperature is controlled within the range of 100-200 °C to avoid serious heat accumulation caused by long-term high temperatures. As shown in Fig. 2, the wall is $300 \times 80 \times 10$ mm, that proves a reasonable interlayer temperature can achieve good forming.

2.3 Characterization Technology

2.3.1 Microstructure Observation. In order to characterize the microstructure of wall parts, all the three-group samples are cut from the middle of the wall parts up-down by electrical discharge cutting and are ground with sandpaper of 80-2000 particle size. Then the ground samples are polished with diamond abrasive paste of 5-0.5 μm particle size. After the sample is corroded by picric acid alcohol solution, the microstructure is observed by a metallographic microscope (Olympus GX71) along the height direction at top, middle, and bottom point of the straight wall. The phase composition of the stacked parts is analyzed by an XRD-7000S x-ray diffractometer. The XRD test samples are the same as the metallographic samples, and they are scanned at 5º/ min within the range of 5º-95º under the target + CuKα, and the scanning step length is 0.4 μm. The microstructure of alloy steel arc additive manufactured straight wall parts is analyzed by the scanning electron microscope equipped with electron backscatter diffraction (EBSD) of Zeiss, Germany.

2.3.2 Test of Mechanical Properties. Since strength and toughness are important properties of structural materials, we follow the ISO148-1: 2016 Standard, and test the mechanical properties of straight wall parts by the uniaxial tensile test and Charpy impact test. The samplings are tested along both the building direction and printing direction. All the three groups of

Fig. 1 Experimental platform for wire and arc additive manufacturing

Table 1 Composition of alloy powder in flux-cored wire (wt.%)

Wire	Cr	Ni	Mo	Ti-Fe	Mn	Al-Mg	B	Ce_2O_3	Fe
1#	9.0	15.0	2.0	3.0	1.0	1.0	0.05	0.5	Bal
2#	9.0	15.0	2.0	4.50	2.0	1.0	0.05	0.5	Bal
3#	9.0	15.0	2.0	6.50	3.0	1.0	0.05	0.5	Bal

Table 2 Composition content of alloy powders (wt.%)

	Cr	Ni	Al	Mg	Nb	C	Ti	Fe	S	P
Ti-Fe	…	…	…	…	…	0.008	60	Bal	0.015	0.02
Al-Mg	…	…	Bal	2	…	0.012	…	…	0.023	0.029

Table 3 Chemical composition of A283GRC steel (wt.%)

C	Mn	Si	S	P
0.14-0.22	0.30-0.65	≤ 0.30	≤ 0.050	≤ 0.045
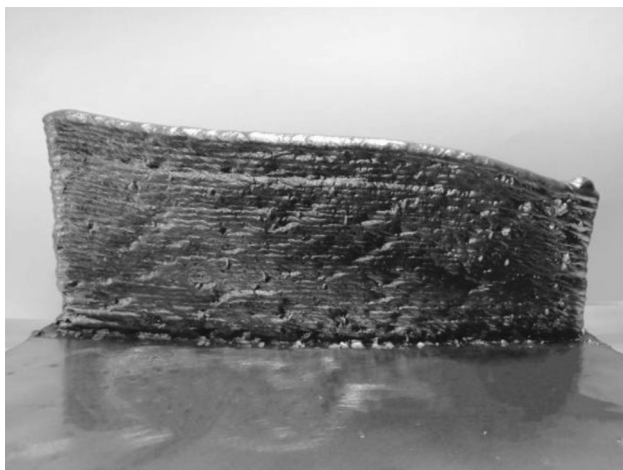
Fig. 2 Wire and arc additive manufactured straight wall parts

parallel samplings are tesed in both directions, and the sampling position is shown in Fig. 3. The fracture of the sampling is observed by the VEGA3 XMU scanning electron microscope (SEM), and element analysis of inclusions is carried out by an energy dispersive spectrometer (EDS) to determine the type of inclusions in the fracture of the tensile specimen.

Also, we test the influence of the thermal cycle and thermal history on the performance of wall parts. To be specific, hardness of straight wall parts made of 1# welding wire along the height direction is tested by a microhardness tester, and hardness of the wall along the building direction is characterized by color distribution. The matrix method is used for the test which proceeds from the top to the bottom of the straight wall. All the three columns are tested one by one. The spacing between indentations is 0.5 mm, the spacing between columns is 1 mm, the loading load was 100 g, and the loading time was 10 s. The microhardness data of each test point is arranged to match the test position.

3. Results and Discussion

3.1 Microscopic Observations

An optical microscope is used to observe the microstructure of the three-group filler wire wall parts, as shown in Fig. 4.
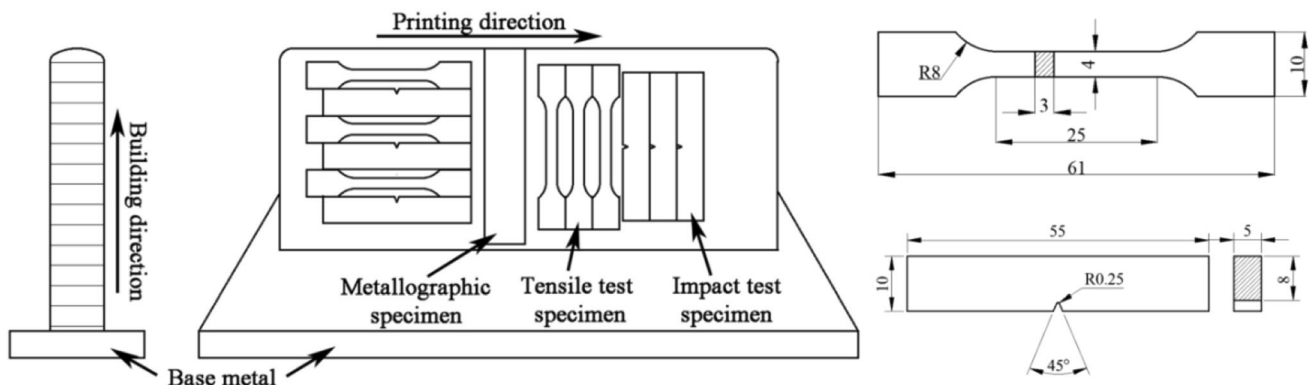

Fig. 3 Sample location and size

During the cooling process the top weld bead is affected by heat accumulation, the cooling rate is reduced and bainite transformation occurs (Ref 23). Owing to addition of strong oxide-forming chemical elements Al, Mg and different contents of Ti, Mn in flux-cored wire metal powder, the top weld bead microstructure contains obvious acicular ferrite. The central weld experiences a complex thermal process which includes the phase transformation process in the solidification process and the phase transformation under the thermal influence of the later stacked weld. When the central weld is initially stacked, heat accumulation in the accumulation body is close to saturation, meanwhile heat input and output reach equilibrium. During the stacking process, the temperature gradient and cooling rate are low (Ref 19), the microstructure after stacking is the same as that of the top weld. In the subsequent accumulation, the subsequent weld bead has a thermal effect on the central microstructure of the straight wall parts, and the solid phase transformation occurs. Due to heat accumulation, the central microstructure of the straight wall parts has tempered bainite transformation during the thermal cycle, and the central microstructure of the alloy steel is transformed into tempered bainite and ferrite.

In order to further determine the phase of the alloy steel stacked straight wall parts in the three groups, the stacked parts are analyzed by XRD. The analysis site to observe the top weld bead and stacked weld bead. The XRD spectra of the alloy steel stacked straight wall parts in the three groups of alloy steel stacked straight wall parts are shown in Fig. 5. Observed from the XRD spectra, the main phase composition of the straight wall parts formed by flux-cored wire is the α-Fe phase with body-centered cubic structure. However, and the characteristic peaks of γ-Fe or carbide are not detected because the amount of γ-Fe or carbide phase in the straight wall parts is below 5%, which is less likely to be distinguished in the XRD test.

The grain boundary distribution of the middle microstructure of the straight wall is shown Fig. 6. The black line represents the large-angle grain boundary whose orientation difference is greater than 15°, and the red line represents the small-angle grain boundary. It is observed that the proportion of the small-angle grain boundary is greater than that of the large-angle grain boundary which is the main boundary between bainite and ferrite. Small-angle grain boundary can play a positive role in hindering crack initiation as well as in the slip of dislocations; large-angle grain boundary can effectively hinder the expansion of brittle cracks and improve toughness of materials (Ref 24). In the EBSD diagram, the grain size of the deposited metal of 2# welding wire is the smallest while that of the deposited metal of 1# and 3# welding wire are relatively large.
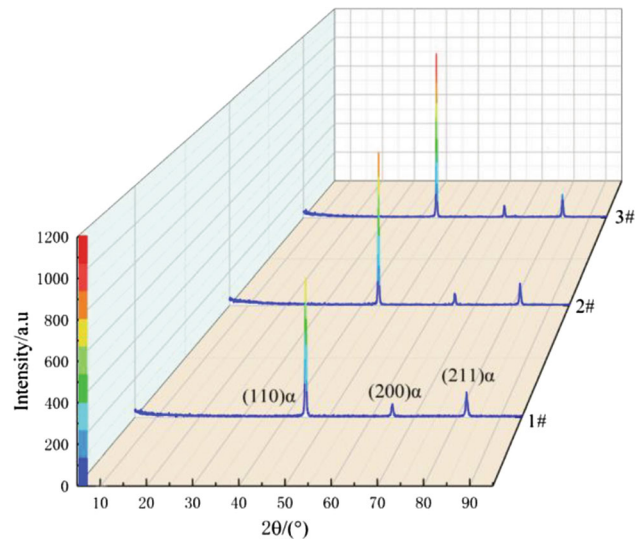

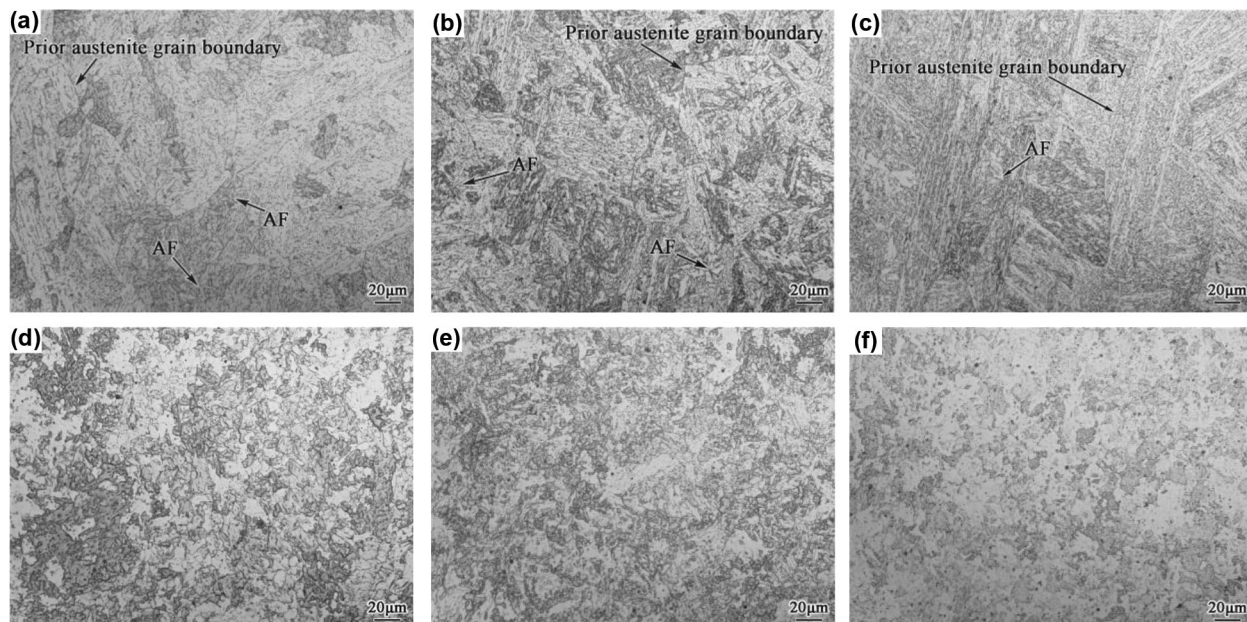**Fig. 5** XRD spectra of alloy steel wall by wire and arc additive manufacturing

Fig. 4 Microstructure: (a) Top weld of 1# wire; (b) Top weld of 2# wire; (c) Top weld of 3# wire; (d) Central weld of 1# wire; (e) Central weld of 2# wire; (d) Central weld of 3# wire
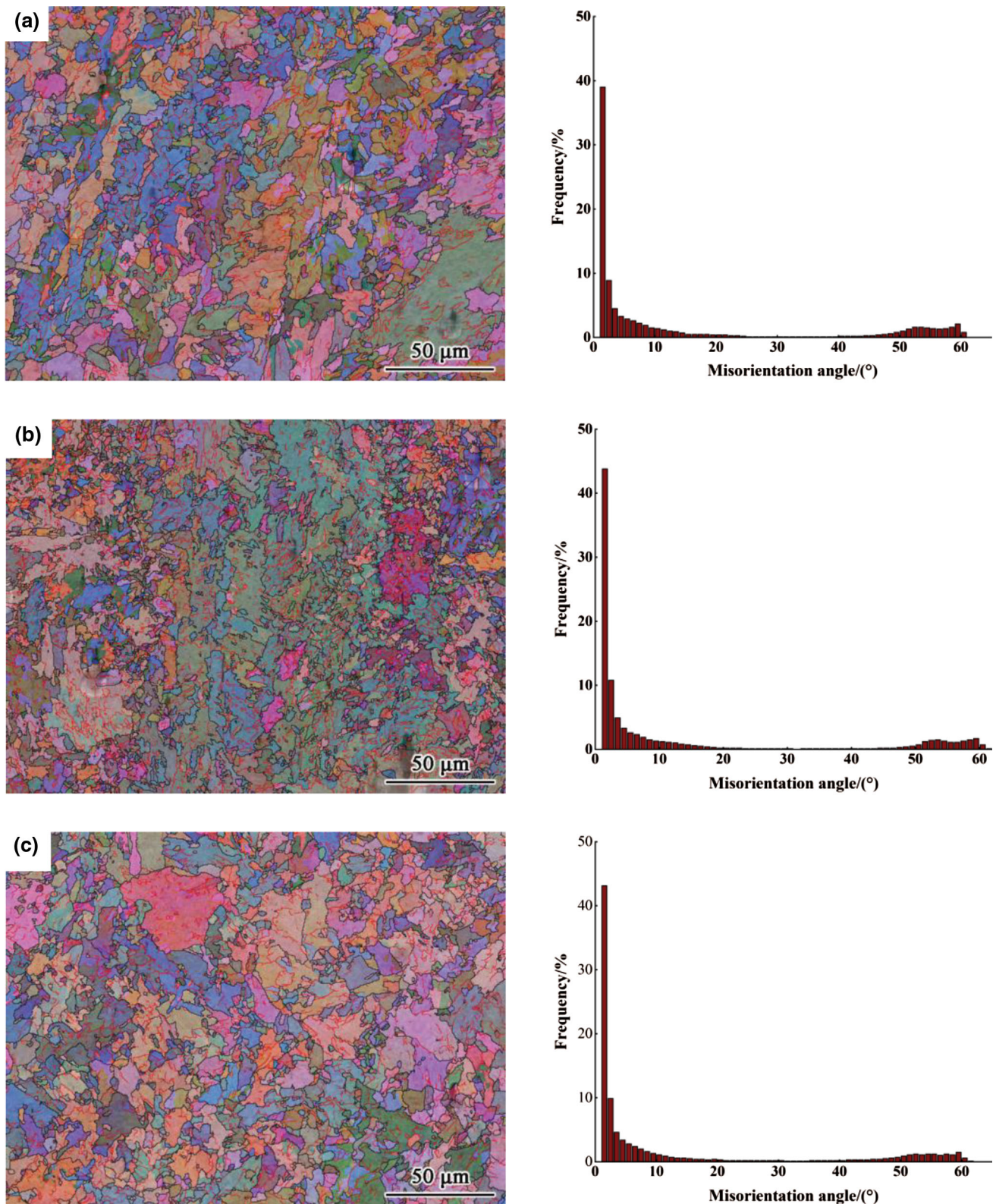
Fig. 6 EBSD map of central of alloy steel wall by wire arc additive manufacturing (a)1# wire; (b) 2# wire; (c) 3# wire

3.2 Microstructure and Performance Transformation of Wall Components

In the process of arc additive manufacturing, the different accumulation sections of the straight wall parts experinece different thermal processes, and the microstructure change to varying degrees. The microstructure of the different regions of the alloy steel arc additive manufactured with 1 # welding wire is shown in Fig. 7, and the observation position is shown in Fig. 7(a). The microstructure of the top weld bead Fig. 7(b) is mainly granular bainite and acicular ferrite. Due to heat
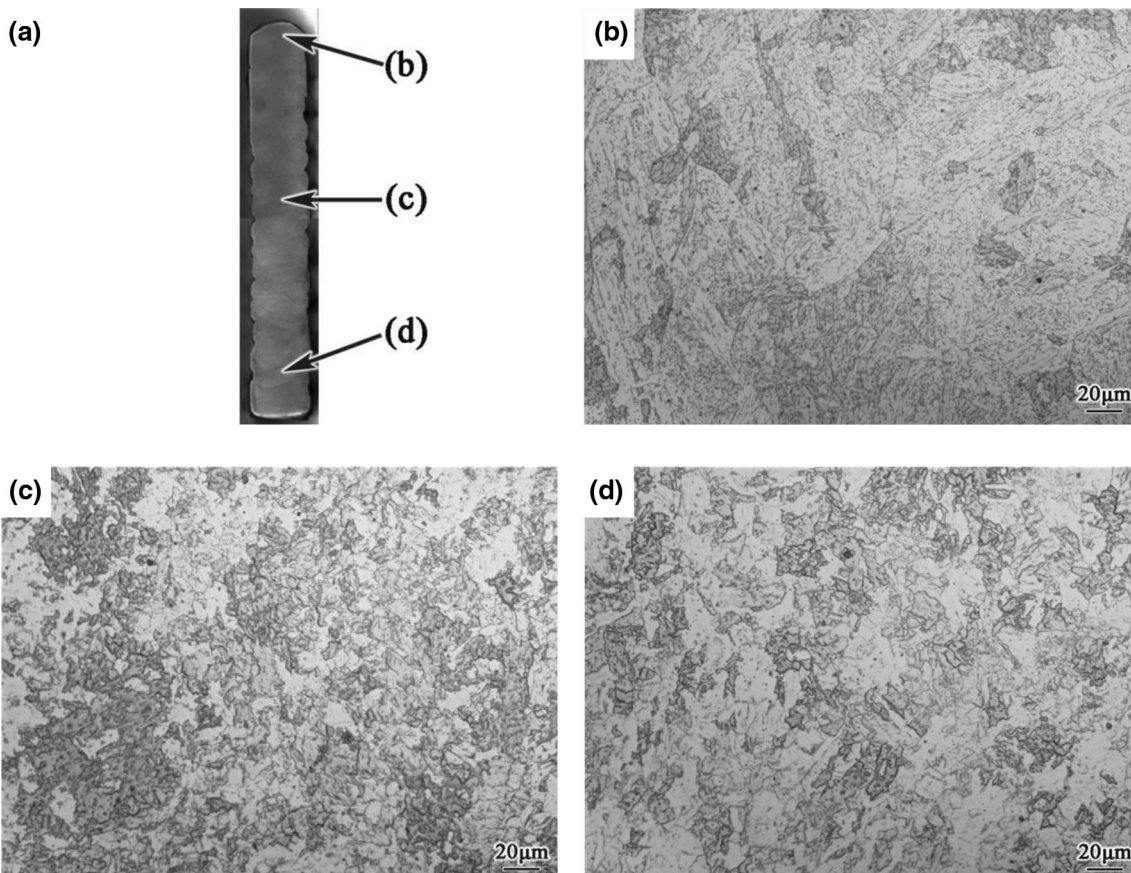
Fig. 7 Microstructure of alloy steel wall by wire arc additive manufacturing. (a)Macro-diagram of sectional; (b) Top of the wall; (c) Central of the wall; (d) Bottom of the wall
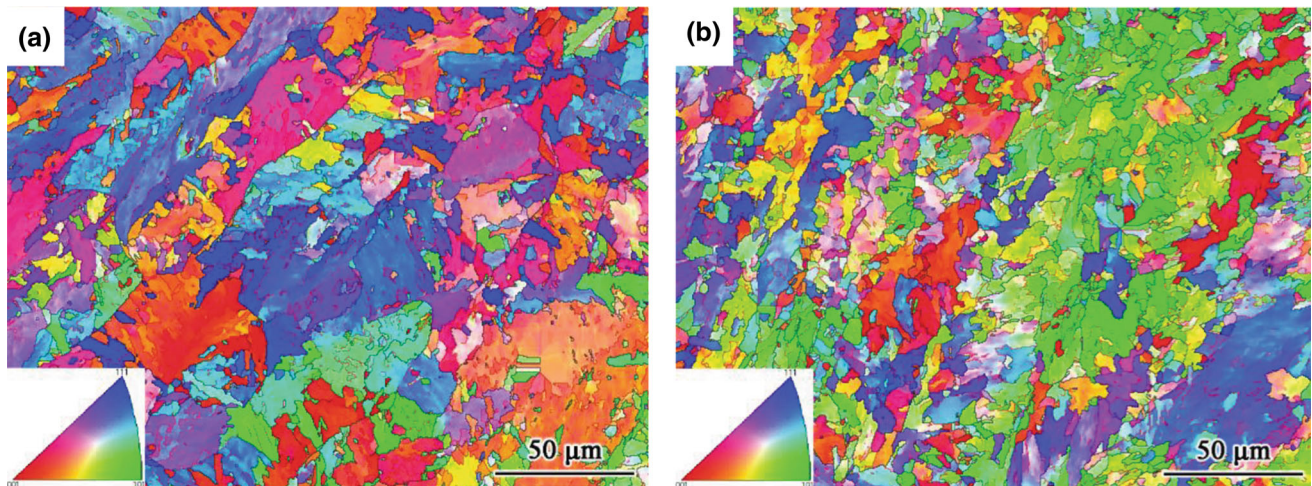

Fig. 8 EBSD diagram of alloy steel by wire arc additive manufacturing top of wall; (b) Central of wall

accumulation during the additive process, the cooling rate of the molten pool decreases, the bainite transformation occurs during the cooling process, and then the top weld bead is dominated by bainite. The microstructure of alloy steel is related to the cooling rate in the process of solid phase transformation. In contrast, martensitic transformation needs a large cooling rate in the traditional welding process. When the single layer is stacked, the cooling rate is fast due to heat dissipation of the substrate, and the martensite transformation occurs in the stacked structure (Ref 25). When the straight wall part is stacked, the new weld bead is stacked. Given manufacturing efficiency and cold crack tendency, the deposited parts cannot be cooled to room temperature., heat accumulation leads to decreasing cooling rate of the weld bead, which cannot meet the requirements of martensite transformation, i.e., the middle-temperature transformation
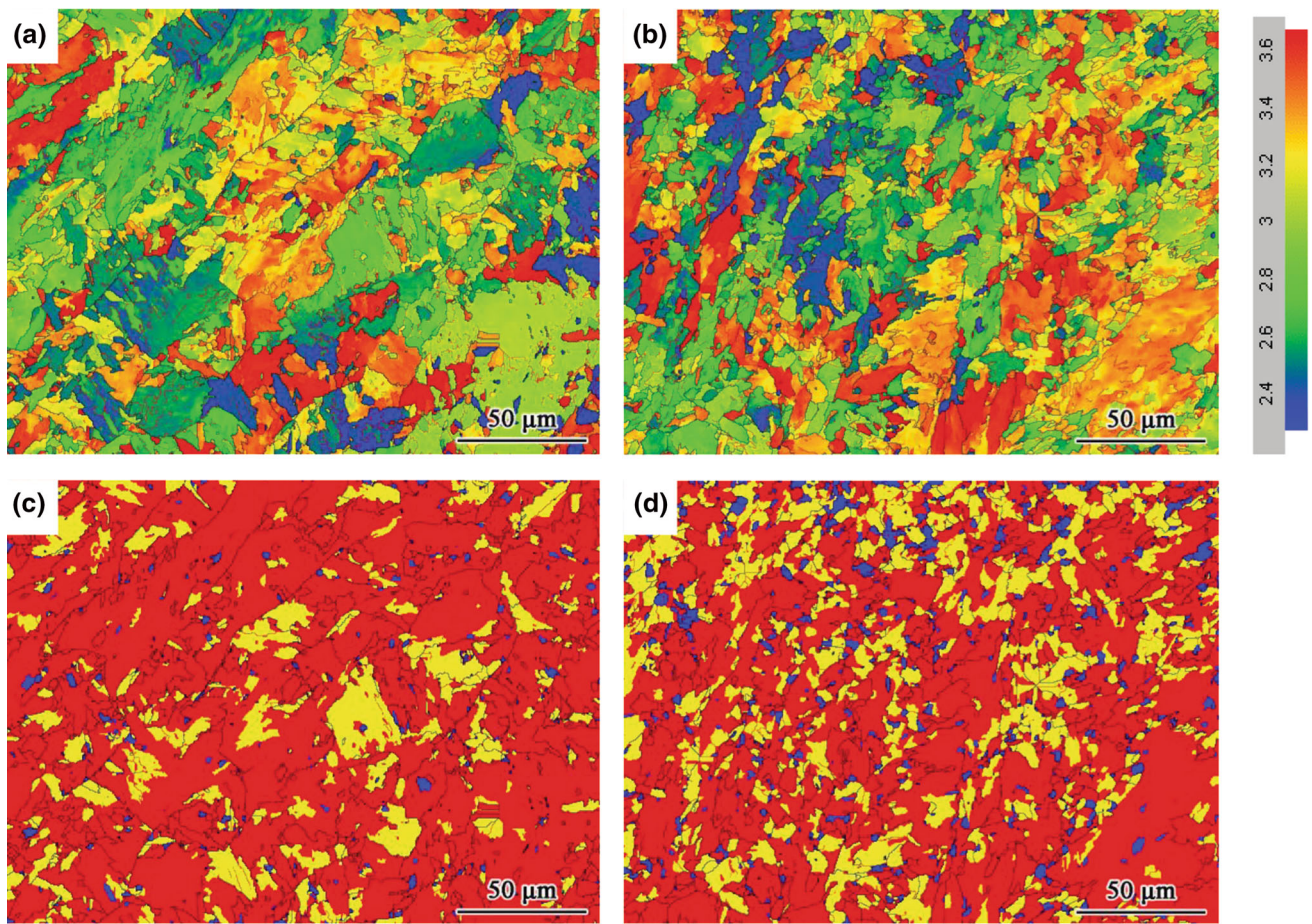
Fig. 9 Taylor factor and recrystallized grain distribution map of top and central of alloy steel wall by wire arc additive manufacturing Taylor factor map: (a) Top of the wall; (b) Central of the wall; recrystallized grain distribution map: (a) Top of the wall; (b) Central of the wall
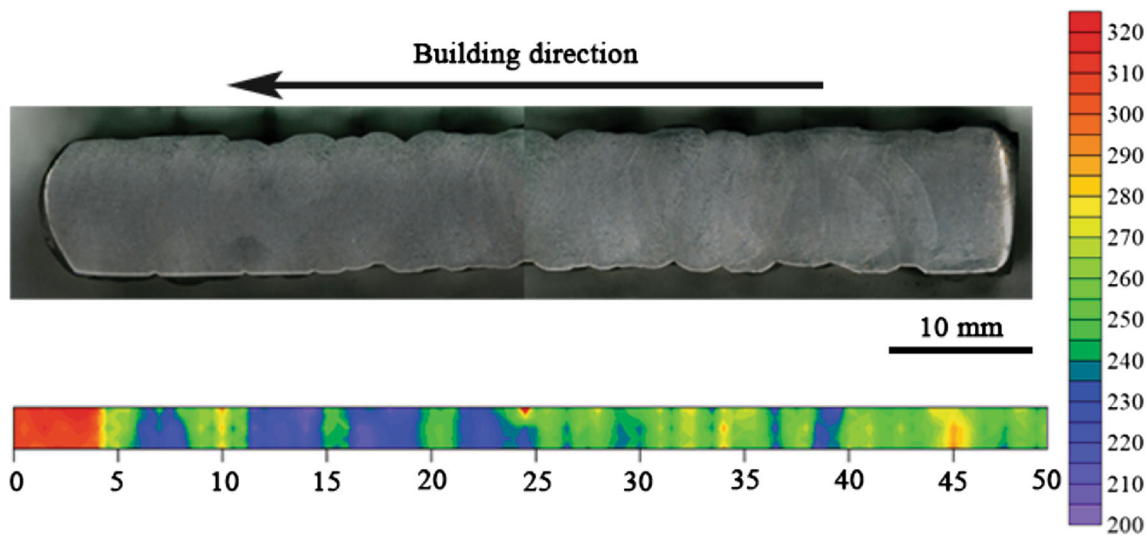

Fig. 10 Microhardness distribution of alloy steel wall by wire arc additive manufacturing

occurs. Therefore, the microstructure of the top weld bead is mainly composed of bainite.

The central weld bead Fig. 7(c) and the bottom weld bead Fig. 7(d) experience the remelting and heating process of the subsequent weld bead, which is similar to the heat-affected zone of alloy steel welding. The microstructure is mainly composed of tempered bainite and massive ferrite. Compared with the middle weld, the thermal process of the bottom weld is more complex and the grain coarsening more serious. Comparing the microstructure of different regions of the straight

wall indicates that the microstructure of the top weld is quite different from that of the middle weld and the bottom weld. Since the raw materials and parameter control remain consistent in the manufacturing process, the difference consists in that each region has experienced different thermal processes which includes different thermal cycles and different cooling rates, resulting in different phase transformation processes in different regions, thus, differences in the microstructure of different sections of the straight wall.

Figure 8 shows the EBSD (Electron Backscatter Diffraction) diagram of the top and middle accumulation structure of the 1# alloy steel arc additive manufactured wall parts. Grains with cubic structure tend to grow along the < 001 > direction because it is parallel to the maximum thermal gradient direction (Ref 26, 27) in most cubic systems during solidification. While the top weld and the middle weld do not show obvious preferred orientation, most grain orientations in the top weld are between [001] and [111]. The grain orientation distribution of the middle weld is more random owing to the complex thermal cycle process, and the random distribution is related to the grain rotation and flow which are caused by convection and process factors during solidification (Ref 28).

Comparing the EBSD images of the top and middle deposited metals indicates that the top weld bead does not have an obvious preferred orientation, but its microstructure is similar to that of the traditional weld microstructure whose grain is coarse and big-sized, whereas the grain size of the middle weld bead is rather smaller. The phase transformation and microstructure development process of the stacked parts manufactured by arc additive are totally different from that in the traditional welding process. The parts manufactured by arc additive have experienced a slower cooling rate. The thermal accumulation and thermal cycle phenomena in the manufacturing process make for more uniform performance of the stacked parts than that of traditional welding.

Figure 9 shows the Taylor factor distribution and recrystallization distribution of the top and middle stacking structure of the 1# alloy steel arc additive manufactured straight wall parts. As an important parameter, Taylor factor is equal to the ratio of the flow stress and the shear stress of the slip system and determines the stress needed to activate the slip system (Ref 29), which means an important relationship between the Taylor factor and the plastic deformation ability of the material. This study shows that the small Taylor factor represents the larger shear stress required for the deformation of the material, and the standard deviation of the Taylor factor is closely related to uniformity of strength distribution in the region. The Taylor factor of the top Fig. 7(a) and the middle Fig. 7(b) welds are calculated, and the average values of the two regions are 3.00 and 3.05, respectively, indicating no significant difference in plasticity even though the top and middle stacking materials experience different thermal processes.

In the traditional welding process, the recovery and recrystallization process of the weld microstructure occurs during the solid phase transformation process and the heat-affected zone. The blue, yellow, and red colors on the recrystallization distribution map, respectively, represent the recrystallized grain, substructure grain, and deformed grain. The proportions of recrystallized grains, sub-structural grains, and deformed grains in the stacking structure of the top weld bead are 2.40, 17.69, and 79.91%, while the proportions of the three types of grain in the middle stacking structure are 6.87%,
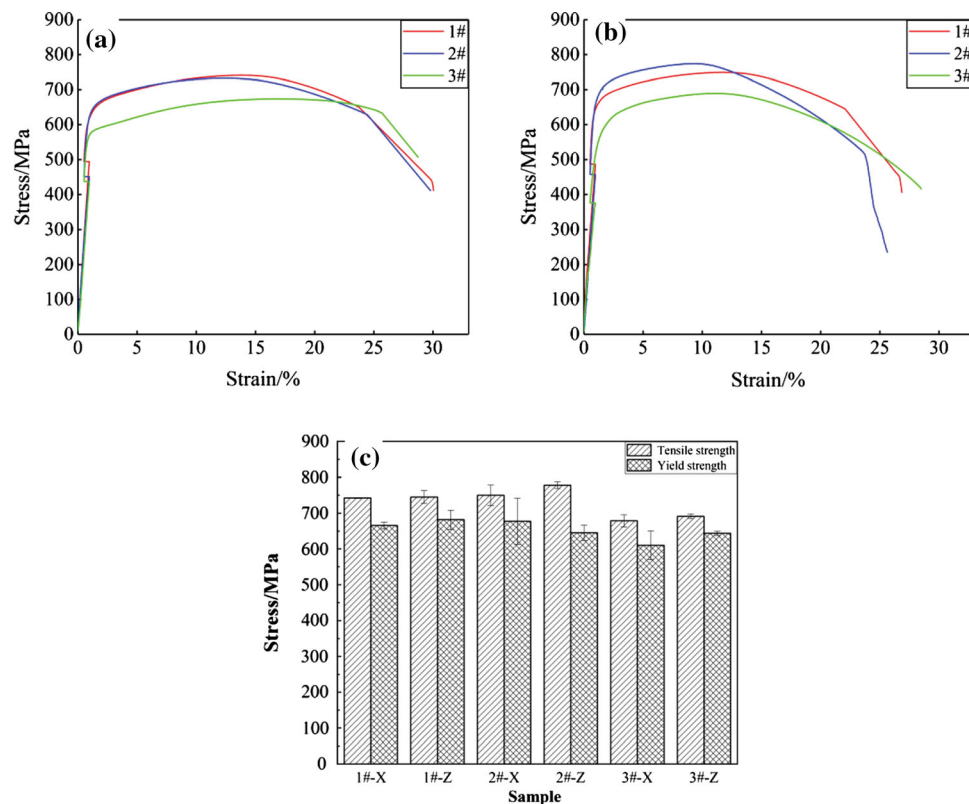

Fig. 11 Strength of the tested sample. (a) The stress-strain curve of stacking direction; (b) The stress-strain curve of printing direction; (c) Tensile test results of alloy steel walls
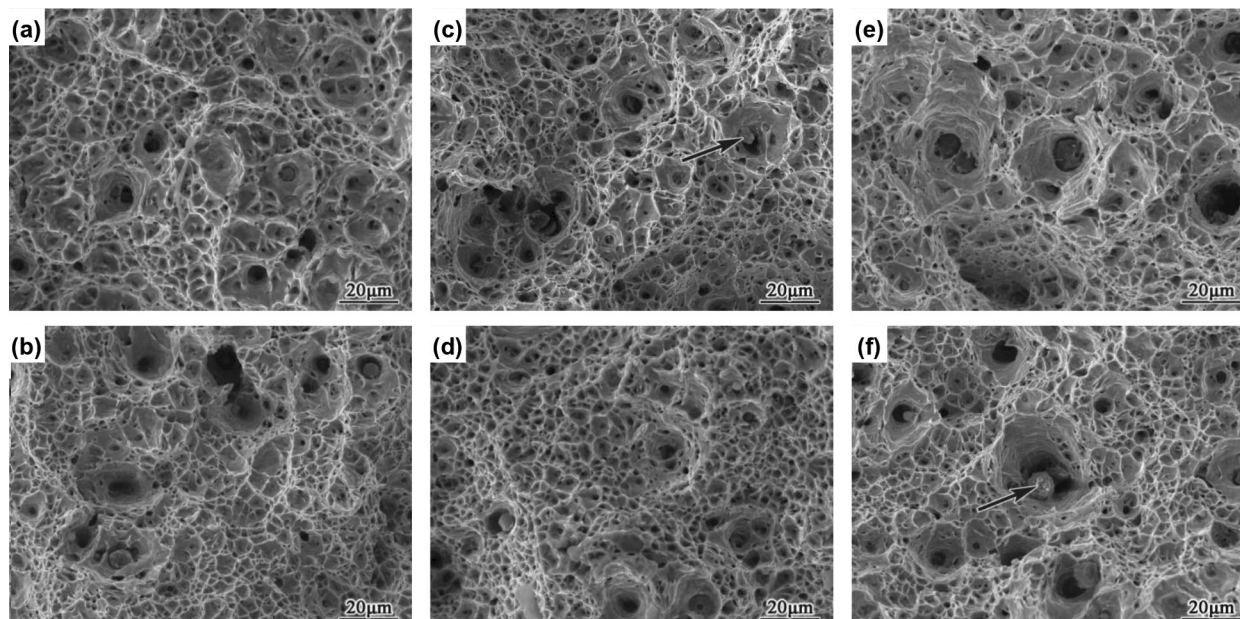
Fig. 12 SEM images of tensile fracture of alloy steel wall by wire arc additive manufacturing vertical direction: (a) 1# wire; (b) 2# wire; (c) 3# wire; crosswise direction: (b) 1# wire; (d) 2# wire; (f) 3# wire

26.89, and 66.24%. The stacking structure is mainly composed of sub-structural grains and deformed grains, and the proportion of deformed grains is the highest. The proportion of recrystallized grains and substructure grains increase with the change of grains in the central stacking structure affected by the subsequent thermal cycle of the weld. Lu et al. (Ref 30) found that the higher proportion of substructures indicated that the material had higher dislocation density, and increase in dislocation density could play a certain strengthening role.

After comparing the microstructure, we conclude that the distribution and morphology of microstructure in different sections of the straight wall parts have changed significantly under influence of thermal cycle and heat accumulation, and the change of microstructure will further improve the mechanical properties of the material. In order to analyze the mechanical properties of different parts of the straight wall parts, the micro Vickers hardness of the straight wall parts manufactured by arc additive of alloy steel is tested along the building direction. Figure 10 shows the microhardness distribution of straight wall parts fabricated by arc additive of Cr-Ni-Mo alloy steel. After the matrix test, hardness changes at different positions are visually displayed by contour plots. Hardness of the top of the wall is the highest, and hardness of the middle and lower parts decreases due to the effect of the welding thermal cycle. In the welding process of alloy high-strength steel, an obvious phenomenon of softening occurs in the heat-affected zone, and the softening degree is related to the austenitizing degree of the heat-affected zone, precipitation of carbides, as well as the aggregating and growing process of carbides. The softening phenomenon is particularly obvious in the incomplete quenching zone between Ac_1 and Ac_3. During the cooling process of the microstructure in this region, the unsaturated austenite decomposes at a higher temperature to form an undissolved ferrite. In the process of arc additive manufacturing, the thermal process of stacking structure is very complex, the block ferrite appears in the middle stacking structure, resulting in decrease in hardness. The microhardness value of additive manufacturing parts is affected by multiple factors. The change of heat input, local composition, weld geometry, and interface affect the phase transformation kinetics, resulting in the change of microstructure and microhardness value. Therefore, the micro-hardness change of straight wall parts along the building direction is closely related to the phase transformation of different parts due to different thermal processes.

3.3 Uniaxial Tensile Tests

In order to examine the effect of Ti and Mn contents on the tensile properties of alloy steel straight wall parts, the uniaxial tensile properties of the three groups of wall parts along the construction direction and printing direction are tested. The tensile test results are summarized in Fig. 11. With increase in Ti and Mn contents, the strength of wall components along the building direction and the printing direction show a trend of increase followed by decrease. As shown in Fig. 6, the microstructure refinement of wall components made by 2# welding wire is the most obvious. According to Hall-Page law, the strength of the material improves with fine-grain strengthening, but the degree of refinement is not large. When the contents of Ti and Mn are the largest, the strength of the wall components is the lowest. The trend of performance change indicates that the strength of wall parts is not affected by any single factor.

Therefore, we attempt at the causes for the strength change of the wall parts with the tensile specimens after a fracture. Figure 12 displays the fracture surface of the wall parts after the tensile test. Addition of tensile Ti and Mn causes inclusion with large dimples of different sizes in the fracture. With the increase in Ti and Mn contents, the number of inclusions in the fracture increases too.

Figure 13 shows the EDS analysis of the particles at the dimple in the tensile fracture, and the test position is shown by the arrow in Fig. 12. The chemical composition indicates two kinds of inclusions in the fracture of tensile specimens. One
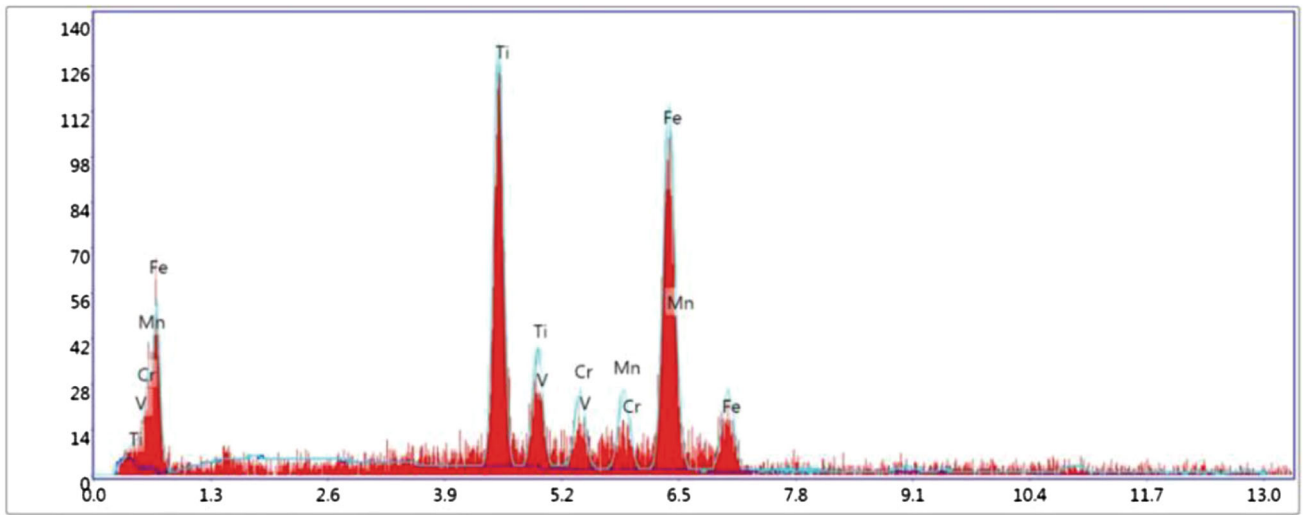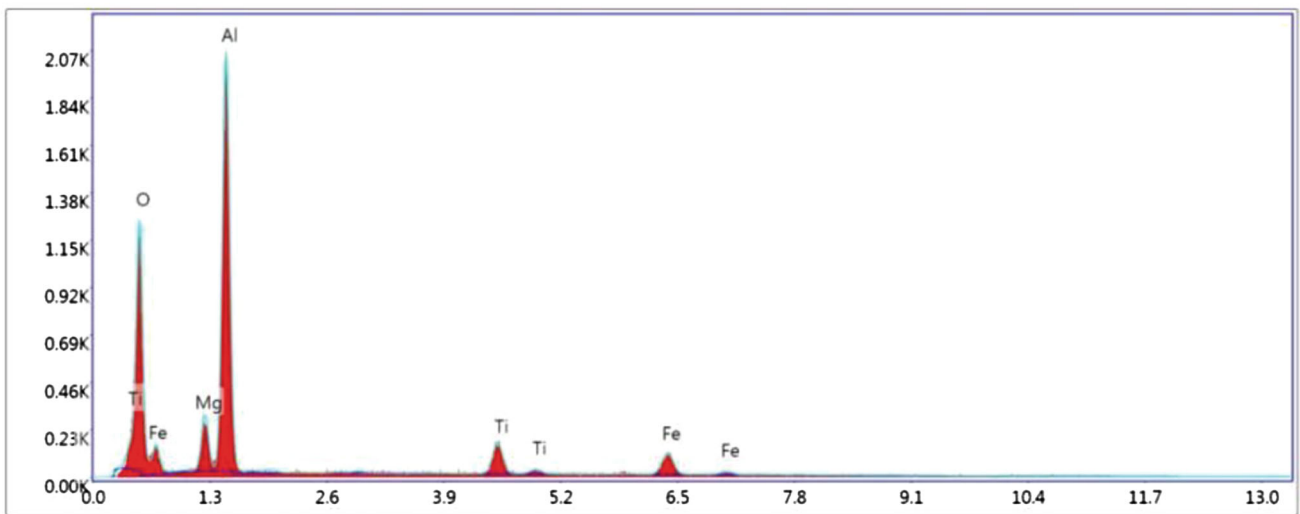
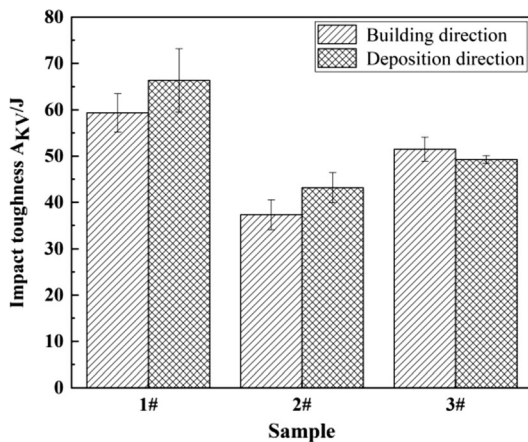**Fig. 13** EDS of inclusion particle in tension fracture

Fig. 14 Impact energy of tensile of alloy steel wall by wire arc additive manufacturing

kind is mainly composed of Fe, Ti, Mn, O and other chemicals, and the other kind is mainly composed of Al, Mg, O and other elements. Therefore, the chemical composition clarify two kinds of inclusions: Al-Mg oxide inclusions and Ti-Mn composite inclusions. These inclusions promote heterogeneous nucleation to the nucleation core in the solidification process and affect grain refinement. At the same time, the inclusions cause the phenomenon of stress concentration for the material in the tensile process so that the actual stress of the material is greater than the external force, thus breaking at a low-stress level, which may lead to decreasing strength of the wall parts (Fig. 14).

3.4 Charpy Impact Tests

When Ti and Mn contents increase, the impact absorption energy of straight wall parts decreases, and Ti and Mn elements form inclusions in the deposited metal. In the tensile fracture

observation, an increase in Ti and Mn contents leads to an increase in the number and density of inclusions in the deposited metal which also contains oxide particles formed by Al elements. The increased number of inclusion particles leads to discontinuity of the material matrix and decreases the material's capability to resist crack propagation, which further decreases the impact absorption energy.

4. Conclusions

This study discusses the arc additive manufacturing of alloy steel made by flux-cored wires of different compositions, focusing on the effect of alloy chemical contents on the microstructure and mechanical properties of wall components produced by arc additive manufacturing, and exploring the microstructure evolution of wall components caused by the thermal cycle. The conclusions are in the following:

(1) The preferential growth is not observed in the top weld bead, and recovery and recrystallization occurr in the middle weld bead. The top weld bead and the middle weld bead are equally capable of resisting plastic deformation.

(2) Excessive Ti and Mn element addition causes inclusion particles to agglomerate. When the inclusion size increases, the number of effective heterogeneous nucleation cores decreases.

(3) Grain refinement avoids coarse columnar crystals, so the mechanical properties of the wall do not show anisotropy.

(4) With increase in Ti and Mn contents, the strength of wall components along the building direction and the printing direction show a trend of increase followed by decrease,and the impact absorption energy of straight wall parts decreases.

References

1. T.A. Rodrigues, V. Duarte, R.M. Miranda, T.G. Santos, and J.P. Oliveira, Current Status and Perspectives on Wire and Arc Additive Manufacturing (WAAM), *Materials*, 2019, **12**(7), p 1121.

2. J. C Najmon, S. Raeisi, and A. Tovar. Review of Additive Manufacturing Technologies and Applications in the Aerospace Industry. Additive Manufacturing for the Aerospace Industry 7-31 (2019).

3. A. Suárez, E. Aldalur, F. Veiga, T. Artaza, I. Tabernero, and A. Lamikiz, Wire arc Additive Manufacturing of an Aeronautic Fitting with Different Metal Alloys: From the Design to the Part, *J. Manuf. Process.*, 2021, **64**, p 188-197.

4. Z. Pan, D. Ding, B. Wu, D. Cuiuri, H. Li, and J. Norrish. Arc Welding Processes for Additive Manufacturing: A Review. Transactions on Intelligent Welding Manufacturing 3-24. (2018).

5. B. Wu, Z. Pan, D. Ding, D. Cuiuri, H. Li, J. Xu, and J. Norrish, A Review of the Wire Arc Additive Manufacturing of Metals: Properties, Defects and Quality Improvement, *J. Manuf. Process.*, 2018, **35**, p 127-139.

6. D. Ding, Z. Pan, D. Cuiuri, and H. Li, Wire-Feed Additive Manufacturing of Metal Components: Technologies, Developments and Future Interests, *Int. J. Adv. Manuf. Technol.*, 2015, **81**(1), p 465-481.

7. J.L. Prado-Cerqueira, A.M. Camacho, J.L. Diéguez, Á. Rodríguez-Prieto, A.M. Aragón, C. Lorenzo-Martín, and Á. Yanguas-Gil, Analysis of Favorable Process Conditions for the Manufacturing of Thin-Wall Pieces of Mild Steel Obtained by Wire and Arc Additive Manufacturing (WAAM), *Materials*, 2018, **11**(8), p 1449.

8. C.V. Haden, G. Zeng, F.M. Carter III., C. Ruhl, B.A. Krick, and D.G. Harlow, Wire and Arc Additive Manufactured Steel: Tensile and Wear Properties, *Addit. Manuf.*, 2017, **16**, p 115-123.

9. J. Lin, Y. Lv, Y. Liu, Z. Sun, K. Wang, Z. Li, Y. Wu, and B. Xu, Microstructural Evolution and Mechanical Property of Ti-6Al-4V Wall Deposited by Continuous Plasma Arc Additive Manufacturing Without Post Heat Treatment, *J. Mech. Behave. Biomed. Mater.*, 2017, **69**, p 19-29.

10. M. Dinovitzer, X. Chen, J. Laliberte, X. Huang, and H. Frei, Effect of Wire and Arc Additive Manufacturing (WAAM) Process Parameters on Bead Geometry and Microstructure, *Addit. Manuf.*, 2019, **26**, p 138-146.

11. P. Kazanas, P. Deherkar, P. Almeida, H. Lockett, and S. Williams, Fabrication of Geometrical Features Using Wire and Arc Additive Manufacture, *Proceed. Inst. Mech. Eng.*, 2012, **226**(6), p 1042-1051.

12. J.J. Lewandowski and M. Seifi, Metal Additive Manufacturing: A Review of Mechanical Properties, *Annu. Rev. Mater. Res.*, 2016, **46**, p 151-186.

13. M. Liberini, A. Astarita, G. Campatelli, A. Scippa, F. Montevecchi, G. Venturini, M. Durante, L. Boccarusso, F.M. Minutolo, and A. Squillace, Selection of Optimal Process Parameters for Wire Arc Additive Manufacturing, *Procedia CIRP*, 2017, **62**, p 470-474.

14. V.V. Pogorelko, and A.E. Mayer, Tensile Strength of Al Matrix with Nanoscale Cu, Ti and Mg Inclusions, *J. Phys. Conf. Ser.*, 2016, **774**(1), p 012034.

15. W. Ou, T. Mukherjee, G.L. Knapp, Y. Wei, and T. DebRoy, Fusion Zone Geometries, Cooling Rates and Solidification Parameters During Wire Arc Additive Manufacturing, *Intern. J. Heat Mass Transf.*, 2018, **127**, p 1084-1094.

16. J. Xiong, Y. Li, R. Li, and Z. Yin, Influences of Process Parameters on Surface Roughness of Multi-Layer Single-Pass Thin-Walled Parts in GMAW-Based Additive Manufacturing, *J. Mater. Process. Technol.*, 2018, **252**, p 128-136.

17. T. Wang, Y. Zhang, Z. Wu, and C. Shi, Microstructure and Properties of Die Steel Fabricated by WAAM Using H13 Wire, *Vacuum*, 2018, **149**, p 185-189.

18. P. Dirisu, S. Ganguly, A. Mehmanparast, F. Martina, and S. Williams, Analysis of Fracture Toughness Properties of Wire+ Arc Additive Manufactured High Strength Low Alloy Structural Steel Components, *Mater. Sci. Eng. A*, 2019, **765**, p 138-285.

19. L. Sun, F. Jiang, R. Huang, D. Yuan, C. Guo, and J. Wang, Microstructure and Mechanical Properties of Low-Carbon High-Strength Steel Fabricated by Wire and Arc Additive Manufacturing, *Metals*, 2020, **10**(2), p 216.

20. A.S. Yildiz, K. Davut, B. Koc, and O. Yilmaz, Wire Arc Additive Manufacturing of High-Strength Low Alloy Steels: Study of Process Parameters and their Influence on the Bead Geometry and Mechanical Characteristics, *Inter. J. Adv. Manuf. Technol.*, 2020, **108**(11), p 3391-3404.

21. B. Wu, Z. Pan, D. Ding, D. Cuiuri, H. Li, and Z. Fei, The Effects of Forced Interpass Cooling on the Material Properties of Wire Arc Additively Manufactured Ti6Al4V Alloy, *J. Mater. Process. Technol.*, 2018, **258**, p 97-105.

22. X. Wang, C.H. Zhang, X. Cui, S. Zhang, J. Chen, and J.B. Zhang, Microstructure and Mechanical Behavior of Additive Manufactured Cr-Ni-V Low Alloy Steel in Different Heat Treatment, *Vacuum*, 2020, **175**, p 109-216.

23. Y. Ali, P. Henckell, J. Hildebrand, J. Reimann, J.P. Bergmann, and S. Barnikol-Oettler, Wire Arc Additive Manufacturing of Hot Work Tool Steel with CMT Process, *J. Mater. Process. Technol.*, 2019, **269**, p 109-116.

24. J.A. Avila, J. Rodriguez, and P.R. Mei, Ramirez AJ Microstructure and Fracture Toughness of Multipass Friction Stir Welded Joints of API-5L-X80 Steel Plates, *Mater. Sci. Eng. A*, 2016, **673**, p 257-265.

25. S.W. Thompson, D.J.V. Col, and G. Krauss, Continuous Cooling Transformations and Microstructures in a Low-Carbon, High-Strength Low-Alloy Plate Steel, *Metall. Trans. A*, 1990, **21**(6), p 1493-1507.

26. P.C. Collins, D.A. Brice, P. Samimi, I. Ghamarian, and H.L. Fraser, Microstructural Control of Additively Manufactured Metallic Materials, *Annu. Rev. Mater. Res.*, 2016, **46**, p 63-91.

27. J. Liu, R.L. Davidchack and H.B. Dong, Molecular Dynamics Calculation of Solid-Liquid Interfacial Free Energy and its Anisotropy During Iron Solidification, *Comput. Mater. Sci.*, 2013, **74**, p 92-100.

28. L. Thijs, M.L. Sistiaga, R. Wauthle, Q. Xie, J.P. Kruth, and J. Van Humbeeck, Strong morphological and crystallographic texture and resulting yield strength anisotropy in selective laser melted tantalum, *Acta Mater.*, 2013, **61**(12), p 4657-4668.

29. E. Bagherpour, F. Qods, R. Ebrahimi, and H. Miyamoto, Microstructure and Texture Inhomogeneity After Large Non-Monotonic Simple Shear Strains: Achievements of Tensile Properties, *Metals*, 2018, **8**(8), p 583.

30. J. Lu, X. Wu, Z. Liu, X. Chen, B. Xu, Z. Wu, and S. Ruan, Microstructure and Mechanical Properties of Ultrafinegrained Copper Produced Using Intermittent Ultrasonic-Assisted Equal-Channel Angular Pressing, *Metal. Mater. Trans. A*, 2016, **47**, p 4648-4658.